TECHNICAL ADVANCE

COVID-19 Lung CT Image Segmentation Using Deep Learning Methods: UNET Vs. SegNET

Adnan Saood[1] and Iyad Hatem[2*]

Abstract

Background: Currently, there is an urgent need for efficient tools to assess in the diagnosis of COVID-19 patients. In this paper, we present feasible solutions for detecting and labeling infected tissues on CT lung images of such patients. Two structurally-different deep learning techniques, SegNet and UNET, are investigated for semantically segmenting infected tissue regions in CT lung images.

Methods: We propose to use two known deep learning networks, SegNet and UNET, for image tissue classification. SegNet is characterized as scene segmentation network and UNet as a medical segmentation tool. Both networks were exploited as binary segmentors to discriminate between infected and healthy lung tissue, and as multi-class segmentors to learn the infection type on the lung. Each network is trained using 72 data images, validated on 10 images and tested against the left 18 images. Several statistical scores are calculated for the results and tabulated accordingly.

Results: The results show the superior ability of SegNet in classifying infected/non-infected tissues compared to the other methods (with 0.95 mean accuracy), while the UNET shows better results as a multi-class segmentor (with 0.91 mean accuracy).

Conclusion: Semantically segmenting CT scan images of COVID-19 patients is a crucial goal because it would not only assist in disease diagnosis , but also help in quantifying the severity of the disease ,and hence, prioritize the population treatment accordingly. We propose computer-based techniques that prove to be reliable as detectors for infected tissue in lung CT scans. The availability of such a method in today's pandemic would help automate, prioritize, fasten, and broaden the treatment of COVID-19 patients globally.

Keywords: COVID-19; pneumonia; SegNet; UNET; Computerized Tomography; Semantic Segmentation

Background

COVID-19 is a widespread disease causing thousands of deaths daily. Early diagnosis of this disease proved to be one of the most effective methods for infection tree pruning [1]. The large number of COVID-19 patients is rendering health care systems in many countries overwhelmed. Hence, a trusted automated technique for identifying and quantifying the infected lung regions would be quiet advantageous.

Radiologists have identified three types of irregularities related to COVID-19 in Computed Tomography (CT) lung images: (1) Ground Glass Opacification (GGO), (2) Consolidation, and (3) Pleural Effusion [2], [3]. Developing a tool for semantically segmenting medical lung images of COVID-19 patients would contribute and assess in quantifying those three irregularities. It would help the front-liners of the pandemic to better manage the situation of overloaded hospitals.

Deep learning (DL) has become a very popular method for constructing netwoks capable of successfully modeling higher-order systems to achieve human-like performance. Tumors have been direct targets for DL-assisted segmentation of medical images. In [4], a lung cancer screening tool was implemented using DL structures aiming to lower the false positive rate in lung cancer screening with low-dose CT scans. Also, in [5], researchers attempted to segment brain tumors from MRI images with a hybrid network of `UNET` and `SegNet`, reaching an accuracy of 0.99. Breast tumor was also a target for segmentation in [6] using Generative Adversarial Networks (`GANs`) and Convolutional Neural Networks (`CNNs`) resulting in a mean accuracy of 0.90. Body parts were subject to segmentation

---

[*] Correspondence: iyad.hatem@tishreen.edu.sy

[2] Mechatronics Program for the Distinguished in Tishreen University, Distinction and Creativity Agency, Latakia, SY

Full list of author information is available at the end of the article

also; researchers attempted to segment: kidneys in [7], Lungs in [8, 9], liver in [10], brain tissue in [11] and [12], temporal bones in [13], and arterial walls in [14]. Until today, many research projects have been conducted for COVID-19 detection using DL analysis of medical images such as X-Ray and Computerized Tomography (CT) scans and revealed significant results. However, semantically segmenting those images has been less appealing.

Many DL structures were considered by researchers to detect COVID-19 patients using medical images. A recent study designed a binary classifier `(COVID-19, No information)` and a multi classifier `(COVID-19 , No Information, Pneumonia)` using a `CNN` with X-Ray images as an input, reaching 0.98 for binary classes and 0.87 for a multi-class classifier [15]. Another study employed `Xception` and `ResNet50V2` networks for COVID-19 detection from CT scans, resulting in an accuracy of 0.99 for the target class [16]. References [17, 18, 19, 20, 21] used various DL systems with medical images and obtained results with accuracy values ranging from 0.83 to 0.98.

Few attempts for semantically segmenting medical images of COVID-19 patients were published recently. A study [22] employed a deep `CNN` as a binary segmentor and compared it to other structures (`FCN, UNET, VNET, UNET++`). The authors reached a Sorensen-Dice of 0.73, a sensitivity of 0.75, and a precision score of 0.73. Another usage of DL as a binary segmentation tool was presented in [23]. The study reached a Dice of 0.78, an accuracy of 0.86, and a sensitivity of 0.94. Reference [24] implemented a Fully Convolutional Network (`FCN`) and a `UNET` as binary segmentation tools, their work performed good in terms of precision and accuracy, lesser in terms of recall and Dice score.

Researchers in [25] detailed the design of a novel DNN structures named `Inf-Net` and `Semi-Inf-Net` to semantically segment infected regions and to segment GGO and consolidation, omitting pleural effusion. Their work utilized the same data set that this research is using.

Methods

The Dataset

Images of the dataset used in this work is a collection of the Italian Society of Medical and Interventional Radiology [26]. One hundred one-slice CT scans are provided in a resized 512 × 512 dimensions. Region labels are already compiled into a NIFTI with proper documentation by the author.

In manual labeling, classes pixel count (total number of pixels in a class) and image pixel count (total number of pixels in images that had an instance of a class) show an extensive disparity in representation; the dominant class is larger in order of 1e+3 than the least represented class. See 1. We note here that the class `C0` not only represent the portions of the lungs unaffected by pneumonia, but also the lung-enclosing tissue.

Table 1 Dataset Class Sizes. Pixel Count denotes the total number of pixels of the class, and Image Pixel Count is the total number of pixels of images that had an instance of the class.

Class Name	Metrics	
	Pixel Count	*Image Pixel Count*
C_0	$2.4394E+07$	$2.6214E+07$
C_1	$1.1965E+06$	$2.5166E+07$
C_2	$5.8921E+05$	$2.0447E+07$
C_3	$3.4265E+04$	$6.5536E+06$

The dataset source website offers image masks to segment the lungs. Figure 1 shows images for one sample.

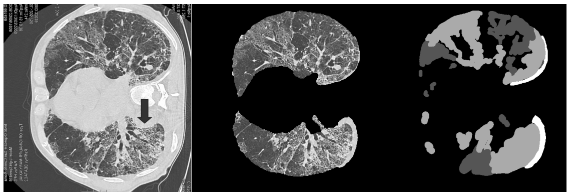

Figure 1 Dataset sample. CT scan (left), masked lungs (middle), and labeled classes (right), where black is class `C0`, dark gray is `C1`, light gray is `C2`, and white is `C3`.

By visual inspection of the datset images, we notice that the ifected areas of the lungs are localized in specific regions. To illustrate the correlation between infected tissue and its elative location, all the labels of the dataset were summed and plotted with hot colormap in Fig. 2. It is clear from the ”accumulation” image that some portions of the lungs are more prone to infection than others. Therefore, the spatial values of pixels tend to be a key feature in this research.

Deep Neural Networks

The overall methodology of semantically segmenting images is to design a structure that extracts features through successive convolutions and uses that information to create a segmentation map as an output. See Fig. 3. In the follwong two paragraphs, we present a brief discription of the two DL networks used in this research.

UNET architecture

The architecture of this network includes two main parts: contractive and expansive. The contracting path consists of several patches of convolutions with filters

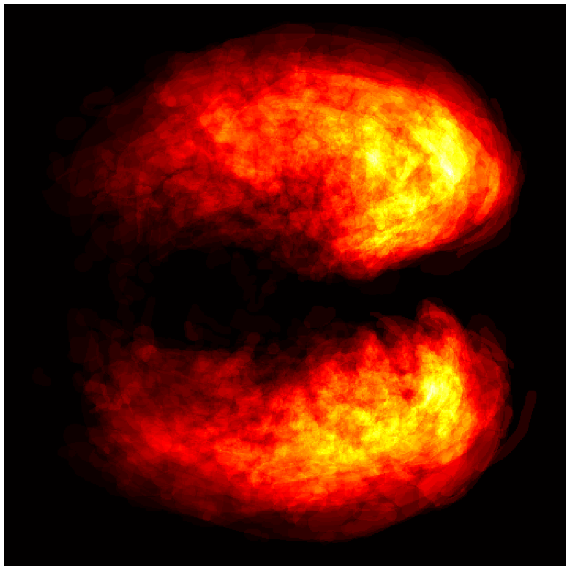

Figure 2 Accumulation of the dataset's labels. All the labels of the dataset were summed up to form a graphic that illustrates the regions of the lungs most prune to infection.

of size 3 × 3, and unity strides in both directions, followed by `ReLU` layers. This path extracts the key features of the input and results a feature vector of a specific length. The second path pulls information from the contractive path via copying and cropping, and from the feature vector via up-convolutions, and generates, by a successive operation, an output segmentation map. The key component of this architecture is the operation linking the first path with the second one, it allows the network to attain highly accurate information from the contractive path to help generate the segmentation mask as close as possible to the intended output. A detailed overview of the architecture can be found in [27].

SegNet Architecture

SegNet is a Deep Neural Network originally designed to model scene segmentors such as road images segmentation. This task requires the network to converge using highly imbalanced datasets since large areas of road images consist of classes as road, sidewalk, and sky, ... etc. The SegNet network is a DNN with an encoder-decoder depth of three. The encoder layers are identical to the convolutional layers of the `VGG16` network. The decoder constructs the segmentation mask by utilizing pooling indices from the max-pooling of the corresponding encoder. The creators removed the fully connected layers to reduce complexity, this reduces the number of parameters of the encoder sector from 1.34e+8 to 1.47e+7. See [28].

Network Training

Training the neural networks is done using the ADAM stochastic optimizer due to its fast convergence rate compared to other optimizers [29]. The input images are resized to 256 × 256 to reduce the training time and also for memory requirements. The one-hundred images dataset is divided into three sets for training, validation, and testing with proportions of 0.72, 0.10, and 0.18 respectively. In spite of the class imbalance discussed earlier, class weights are handed over to the pixel classification layer in the networks. Weights are calculated using median frequency balancing. Each network is trained nine times using different hyperparameters to find the best configuration possible. Table 2 lists the hyperparameters used for training.

Table 2 Hyperparameters used for training the DNNs. Nine experiments for each network with different initial learning rates (ILR) and mini batch sizes.

	SegNet		UNET	
Exp.	ILR	MniBatch	ILR	MiniBatch
1	1e−4	4	1e−4	2
2	1e−4	4	1e−4	2
3	1e−4	4	1e−4	2
4	1e−3	8	5e−4	8
5	1e−3	8	5e−4	8
6	1e−3	8	5e−4	8
7	3e−3	12	1e−3	12
8	3e−3	12	1e−3	12
9	3e−3	12	1e−3	12

The training process was done using the Deep Learning Toolbox version 14.0 in MATLAB R2020a (9.8.0.1323502) in a Windows 10 version 10.0.18363 machine with an INTEL core-i5 9400F and an NVIDIA 1050ti 4GB VRAM GPU using CUDA 10.0.130. Usage of the GPU reduced training times by a factor of 35 on average.

Evaluation Criteria and Procedure

To fully quantify the performance of our models, we utilized five known classification criteria: sensitivity, specificity, G-mean, Sorensen-Dice (aka. F1), and F2 score. The following equations (1) to (5) describe these criteria:

$$\text{sensitivity} = \frac{\text{TP}}{\text{TP} + \text{FN}} \tag{1}$$

$$\text{specificity} = \frac{\text{TN}}{\text{TN} + \text{FP}} \tag{2}$$

$$\text{Sorensen-Dice} = \frac{2 \times \text{TP}}{2 \times \text{TP} + \text{FP} + \text{FN}} \tag{3}$$

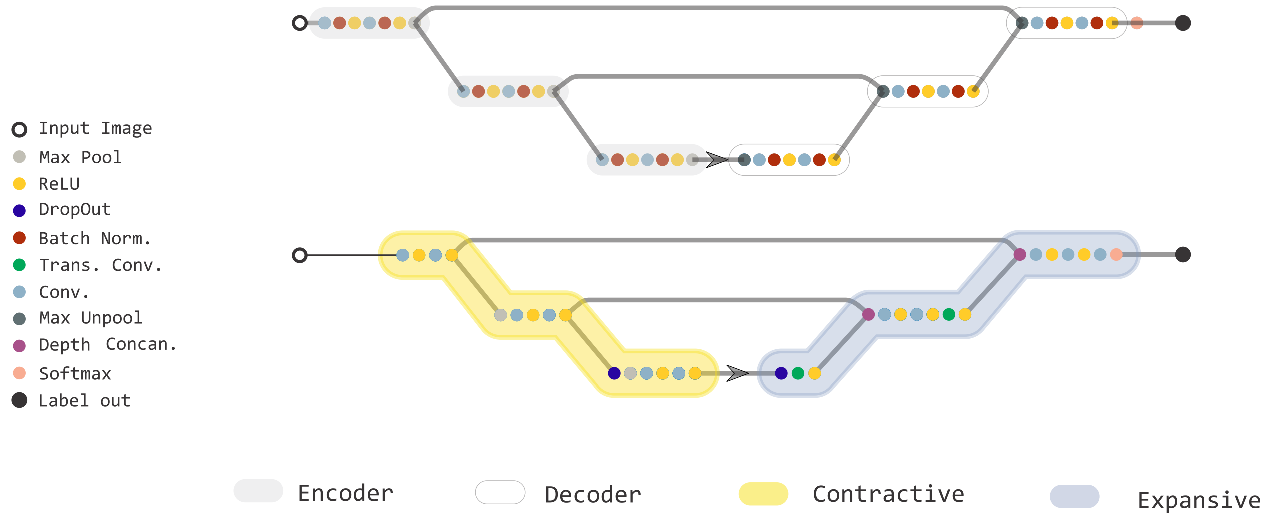

Figure 3 The DNN architectures. The SegNet (top) where the encoder-decoder of the network are illustrated using the gray and white bubbles, and UNET (bottom) where the contractive and expansive layer patches are encapsulated in blue and yellow bubbles.

$$\text{G-mean} = \sqrt{\text{sensitivity} \times \text{specificity}} \tag{4}$$

$$\text{F2-score} = \frac{5 \times \text{Precision} \times \text{Sensitivity}}{4 \times \text{Precision} + \text{Sensitivity}} \tag{5}$$

These criteria are selected because of the dataset imbalance nature discussed in the “Methods” section.

The evaluation was carried out as follows: the global accuracy of the classifier was calculated for each test image and averaged over all the images. Using the mean values of global accuracies, the best experiment of each network were chosen for a *“Class Level”* assessment. Then, statistical scores (1) to (5) were calculated for each class and tabulated properly.

Results

Binary Segmentation

Test images results

Table 3 shows results for both models of binary classifiers after evaluating every experiment of each network. We can see from the results that our networks achieve accuracy values larger than 0.90 in all cases, and 0.954 accuracy in the best case (experiment 4 of the network SegNet). The standard deviation of experiment 4 is 0.029. The second best network is experiment 4 of the UNET architecture with an accuracy of 0.95 and a standard deviation of 0.043.

The best experiment of each architecture is selected for further performance investigation on the class level.

Class Level

Based on the criteria discussed in subsection of the ”Methods” section, the best two networks found in the previous section are evaluated. We can see that the SegNet network surpasses UNET with noticeable margins for all metrics except sensitivity and G-mean, where both networks produce similar results. See table 5

Multi Class Segmentation

Test images results

Similarly, we obtain the best experiment for each multi-classification network. The best experiment of the `SegNet` architecture is number 7, giving an accuracy of 0.907 with a standard deviation of 0.06. We also find that the overall best accuracy of 0.908 is given by the fourth experiment of `UNET` network with a standard deviation of 0.065. All the experiments achieve higher accuracy than 0.8 except for the first three experiments of SegNet. Refer to table 4.

Class level

In the same manner as the binary segmentation results section, the best experiment of each architecture is evaluated as presented in table 6. Both networks struggled to recognize the `C3` class. Nevertheless, they achieve good results for `C1` and `C2`. We also notice the high specificity rate regarding all the classes. The UNET architecture recorded higher values for all parameters except the specificity.

Table 3 Global accuracy metrics of the Test data images calculated for the nine experiments of the UNET and SegNet networks as binary class segmentors. The "plot" columns visualize the mean accuracy and the standard deviation of each experiment

	SegNet				**UNET**			
				plot of mean and σ				plot of mean and σ
Exp.	mean	σ	var	0 → 1 	mean	σ	var	0 → 1 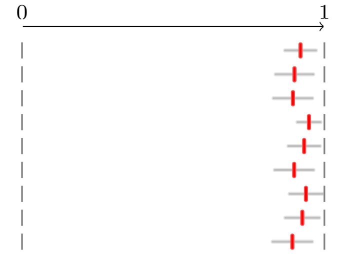
1	0.934	0.053	0.004		0.921	0.056	0.003	
2	0.919	0.061	0.004		0.901	0.067	0.004	
3	0.919	0.066	0.007		0.896	0.069	0.005	
4	**0.954**	0.029	0.004		**0.949**	0.043	0.002	
5	0.940	0.052	0.005		0.933	0.057	0.003	
6	0.947	0.042	0.005		0.900	0.069	0.005	
7	0.941	0.033	0.003		0.939	0.059	0.003	
8	0.935	0.056	0.004		0.927	0.061	0.003	
9	0.948	0.046	0.005		0.894	0.070	0.005	

Table 4 Global accuracy metrics of the Test data images calculated for the nine experiments of the UNET and SegNet networks as multi-class segmentors. The "plot" columns visualize the mean accuracy and the standard deviation of each experiment.

	SegNet				**UNET**			
				plot of mean and σ				plot of mean and σ
Exp.	mean	σ	var	0 → 1 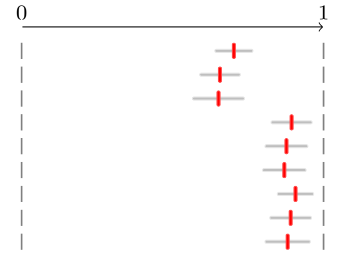	mean	σ	var	0 → 1 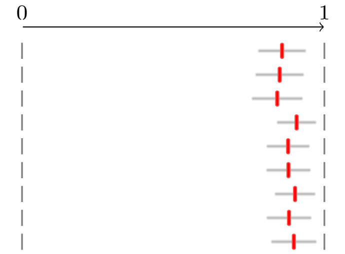
1	0.703	0.063	0.004		0.860	0.079	0.006	
2	0.657	0.067	0.004		0.852	0.080	0.006	
3	0.652	0.086	0.007		0.844	0.084	0.007	
4	0.894	0.068	0.004		**0.908**	0.065	0.004	
5	0.877	0.071	0.005		0.880	0.071	0.005	
6	0.870	0.072	0.005		0.881	0.073	0.005	
7	**0.907**	0.060	0.003		0.903	0.067	0.004	
8	0.891	0.069	0.004		0.883	0.074	0.005	
9	0.881	0.075	0.005		0.899	0.075	0.005	

Table 5 Statistical results for the binary segmentor. SegNet and UNET binary segmentation tools results is terms of sensitivity, specificity, dice, G-mean, and F2 score.

Net.	Sens.	Spec.	Dice	G-mean	F2
SegNet	0.956	**0.9542**	**0.749**	0.955	**0.861**
UNET	**0.964**	0.948	0.733	**0.956**	0.856

Table 6 Statistical results for the multi segmentor. SegNet and UNET multi class segmentation tools results is terms of sensitivity, specificity, dice, G-mean, and F2 score. Matching color rows display the results for the same class.

Net.	Class	**Sens.**	**Spec.**	**Dice.**	**G-mean**	**F2**
SegNet	C_1	0.638	**0.952**	0.479	0.780	0.562
	C_2	0.672	0.965	0.454	0.806	0.564
	C_3	0.574	0.988	0.121	0.753	0.231
UNET	C_1	**0.804**	0.930	**0.483**	**0.865**	**0.636**
	C_2	**0.694**	**0.983**	**0.597**	**0.826**	**0.652**
	C_3	**0.684**	**0.993**	**0.225**	**0.824**	**0.377**

Discussion

Binary classification problem

It can be referred from table 6 that `SegNet` outperforms `UNET` architecture by a noticeable margin. Both networks have an exceptionally high true positive count for the "Not Infected" class. The results state in a quantifiable manner how reliable is the DNN models in distinguishing between the non-infected and infected classes, i.e. ill portions of the lungs. Further experiments involving a larger dataset is likely to confirm this. The high sensitivity (0.956) and specificity (0.945) of the best network (SegNet) indicate its goodness in modeling a trained radiologist for the task in hand.

Regarding the standard deviation of the results demonstrated in table 3, the values ranged from 0.060 to 0.086. These low values indicate highly consistent accuracies in the test partition of the dataset.

The results of our SegNet show enhancements over the results presented in [25] in terms of the Dice metric, specificity, and sensitivity. As well, the UNET outperforms it only in terms of sensitivity. For sure, both works utilize the same dataset. SegNet also surpasses the COVID-NET architecture proposed in [22] in sensitivity and Dice metrics. A more detailed comparison is necessary to further generalize this result.

Multi Class problem

Table 6 shows how good the UNET is in segmenting the Ground Glass Opacification and the Consolidation. The UNET produced moderate results in segmenting the pleural effusion; a Dice of 0.23 and F2 score of 0.38 which downplays its role as a reliable tool for pleural effusion segmentation.

It should be noted here that increasing the mini-batch size has a negative effect on the networks performance, further test may lead to a generalized statement regarding this matter.

The `C3` class, as discussed in , is the least represented class in the dataset, and such a result is expected from a multi-class segmentation model constructed using 72 image instances only.

The standard deviation values were, on average, a little higher than the binary segmentors. Yet, they still indicate that the networks are solid performers in terms of accuracy. The high specificity rates clearly state that the models are reliable in identifying non-infected tissue (class `C0`).

Network Feature Visualization

Deep Dream is a method used to visualize the features extacted by the network after the training process [30]. Since the `SegNet` proved to be a reliable segmentor considering its high statistical scores, the generated Deep Dream image should lay out the key features distinguishing each class (`non-infected`, `infected`). We plotted the Deep Dream image in Fig. 4. We can apparently visualize a discerning pattern between the two classes in this image.

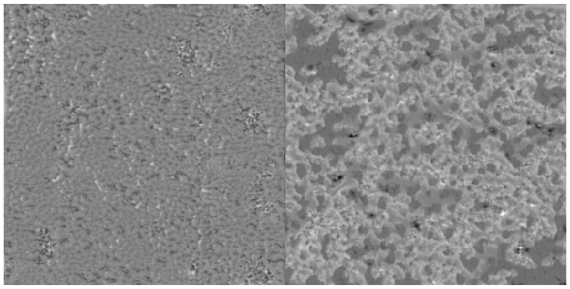

Figure 4 SegNet binary segmentor Deep Dream image. Deep dream image laying out key features the network is using to segment the CT scans. infected tissue (right), non-infected (left).

Conclusions

In this paper, the performance of two deep learning networks (SegNet & UNET) was compared in their ability to detect diseased areas in medical images of the lungs of COVID-19 patients. The results demonstrated the ability of the SegNet network to distinguish between infected and healthy tissues in these images. A comparison of these two networks was also performed in a multiple classification procedure of infected areas in lung images. The results showed the UNET network's ability to distinguish between these areas. The results obtained in this paper represent promising prospects for the possibility of using deep learning to assist in an objective diagnosis of COVID-19 disease through CT images of the lung.

List of abbreviations

GGO: Ground Glass Opacification; DL: Deep Learning; DNN: Deep Neural Network; COVID-19: COrona VIrus Disease 2019; CT: Computerized Tomography; CNN: Convolutional Neural Network; GAN: Generative Adversarial Networks; FCN: Fully Convolutional Network

Declarations

Ethics approval and consent to participate

The dataset used in this work is openly accessible and free to the public. No direct interaction with a human or animal entity was conducted in this work.

Consent for publication

Not applicable for this paper.

Availability of data and materials

The data is openly accessible in [26], and the networks used in this work are freely available in `https://github.com/adnan-saood/COVID19-DL`.

Competing interests

The authors declare that they have no competing interests.

Funding

This research did not require funding.

Authors' contributions

IH proposed the research idea, the dataset, and the overall methodology. AS developed the methods and performed the experiments, collected the results and drafted the paper. Both authors drew the conclusions.

Acknowledgements

Data for this study come from the Italian Society of Medical and Interventional Radiology [26]

Author details

[1]Mechatronics Program for the Distinguished in Tishreen University, Distinction and Creativity Agency, Latakia, SY. [2]Mechatronics Program for the Distinguished in Tishreen University, Distinction and Creativity Agency, Latakia, SY.

References

1. meizhu chen, changli tu, Tan C, Zheng X, xiaohua wang, jian wu, et al. Key to successful treatment of COVID-19: accurate identification of severe risks and early intervention of disease progression. 2020 Apr;.
2. Shi H, Han X, Jiang N, Cao Y, Alwalid O, Gu J, et al. Radiological findings from 81 patients with COVID-19 pneumonia in Wuhan, China: a descriptive study. The Lancet Infectious Diseases. 2020 Apr;20(4):425–434.
3. Ye Z, Zhang Y, Wang Y, Huang Z, Song B. Chest CT manifestations of new coronavirus disease 2019 (COVID-19): a pictorial review. European Radiology, Mar. 2020;.
4. Causey JL, Guan Y, Dong W, Walker K, Qualls JA, Prior F, et al.. Lung cancer screening with low-dose CT scans using a deep learning approach; 2019. Available from: https://arxiv.org/abs/1906.00240.
5. Daimary D, Bora MB, Amitab K, Kandar D. Brain Tumor Segmentation from MRI Images using Hybrid Convolutional Neural Networks. Procedia Computer Science. 2020;167:2419–2428.
6. Singh VK, Rashwan HA, Romani S, Akram F, Pandey N, Sarker MMK, et al. Breast tumor segmentation and shape classification in mammograms using generative adversarial and convolutional neural network. Expert Systems with Applications. 2020 Jan;139:112855.
7. Zhao W, Jiang D, Queralta JP, Westerlund T. MSS U-Net: 3D segmentation of kidneys and tumors from CT images with a multi-scale supervised U-Net. Informatics in Medicine Unlocked. 2020;19:100357.
8. Skourt BA, Hassani AE, Majda A. Lung CT Image Segmentation Using Deep Neural Networks. Procedia Computer Science. 2018;127:109–113.
9. Huidrom R, Chanu YJ, Singh KM. Automated Lung Segmentation on Computed Tomography Image for the Diagnosis of Lung Cancer. CyS. 2018 9;22(3).

10. Almotairi S, Kareem G, Aouf M, Almutairi B, Salem MAM. Liver Tumor Segmentation in CT Scans Using Modified SegNet. Sensors. 2020 Mar;20(5):1516.
11. Kumar P, Nagar P, Arora C, Gupta A. U-SegNet: Fully Convolutional Neural Network based Automated Brain tissue segmentation Tool; 2018. Available from: `https://arXiv.org/abs/1806.04429`.
12. Akkus Z, Kostandy P, Philbrick KA, Erickson BJ. Robust brain extraction tool for CT head images. Neurocomputing. 2020 6;392:189–195.
13. Li X, Gong Z, Yin H, Zhang H, Wang Z, Zhuo L. A 3D deep supervised densely network for small organs of human temporal bone segmentation in CT images. Neural Networks. 2020 4;124:75–85.
14. Yang J, Faraji M, Basu A. Robust segmentation of arterial walls in intravascular ultrasound images using Dual Path U-Net. Ultrasonics. 2019 7;96:24–33.
15. Ozturk T, Talo M, Yildirim EA, Baloglu UB, Yildirim O, Acharya UR. Automated detection of COVID-19 cases using deep neural networks with X-ray images. Computers in Biology and Medicine. 2020 6;121:103792.
16. Rahimzadeh M, Attar A. A modified deep convolutional neural network for detecting COVID-19 and pneumonia from chest X-ray images based on the concatenation of Xception and ResNet50V2. Informatics in Medicine Unlocked. 2020;19:100360.
17. Xu X, Jiang X, Ma C, Du P, Li X, Lv S, et al. A Deep Learning System to Screen Novel Coronavirus Disease 2019 Pneumonia. Engineering. 2020 Jun;.
18. Wang S, Kang B, Ma J, Zeng X, Xiao M, Guo J, et al. A deep learning algorithm using CT images to screen for Corona Virus Disease (COVID-19). 2020 Feb;.
19. Zheng C, Deng X, Fu Q, Zhou Q, Feng J, Ma H, et al. Deep Learning-based Detection for COVID-19 from Chest CT using Weak Label. 2020 Mar;.
20. Apostolopoulos ID, Mpesiana TA. Covid-19: automatic detection from X-ray images utilizing transfer learning with convolutional neural networks. Phys Eng Sci Med. 2020 4;43(2):635–640.
21. Narin A, Kata C, Pamuk Z. Automatic Detection of Coronavirus Disease (COVID-19) Using X-ray Images and Deep Convolutional Neural Networks; 2020. Available from: `https://arxiv.org/abs/2003.10849`.
22. Yan Q, Wang B, Gong D, Luo C, Zhao W, Shen J, et al.. COVID-19 Chest CT Image Segmentation – A Deep Convolutional Neural Network Solution; 2020. Available from: `https://arxiv.org/abs/2004.10987`.
23. Amyar A, Modzelewski R, Ruan S. Multi-task Deep Learning Based CT Imaging Analysis For COVID-19: Classification and Segmentation. Cold Spring Harbor Laboratory, Apr. 2020;21.
24. Voulodimos A, Protopapadakis E, Katsamenis I, Doulamis A, Doulamis N. Deep learning models for COVID-19 infected area segmentation in CT images. Cold Spring Harbor Laboratory. 2020 5;.
25. Fan DP, Zhou T, Ji GP, Zhou Y, Chen G, Fu H, et al. Inf-Net: Automatic COVID-19 Lung Infection Segmentation from CT Images. 2020 Apr;.
26. COVID-19, Medical segmentation;. Available from: `http://medicalsegmentation.com/covid19/`.
27. Ronneberger O, Fischer P, Brox T. U-Net: Convolutional Networks for Biomedical Image Segmentation. In: Lecture Notes in Computer Science. Springer International Publishing; 2015. p. 234–241.
28. Badrinarayanan V, Kendall A, Cipolla R. SegNet: A Deep Convolutional Encoder-Decoder Architecture for Image Segmentation. IEEE Transactions on Pattern Analysis and Machine Intelligence. 2017 Dec;39(12):2481–2495.
29. Kingma DP, Ba J. Adam: A Method for Stochastic Optimization; 2014. Available from: `https://arxiv.org/abs/1412.6980`.
30. Mordvintsev A, Olah C, Tyka M. Inceptionism: Going Deeper into Neural Networks. Google Research; 2015. Archived from the original on 2015-07-03.